Numerical study of the wave impacts generated in a wet dam break

L.E. Dumergue, Stéphane Abadie

- Numerical study of impacts generated in a dam break varying depth and obstacle position
- All types of wave impacts were obtained through this set-up by adjusting the parameters
- Impact pressures one order of magnitude larger than in previous dam break studies
- Wet dam break may be quick and simple way to generate strong wave impacts

Numerical study of the wave impacts generated in a wet dam break

L.E. Dumergue[a], S. Abadie[a]

[a]*Universite de Pau et des Pays de l'Adour, E2S UPPA, SIAME, Anglet, France*

Abstract

This paper focuses on the numerical analysis of the different wave impacts generated in a wet dam break by varying the downstream depth and the position of the obstacle. With this relatively simple set-up, five hundred impacts were simulated, providing a comprehensive dataset covering the four classical impact types : sloshing, flip-through, aerated and broken wave impacts. We determined the dam break parameters for which the flip-trough impacts occur and showed that among all the flip-through impacts, there is one optimum generating a pressure peak larger that the others. Compared to impact pressures recorded or simulated with a dam break flow in most previous studies, the present numerical work reached values one order of magnitude larger. Therefore with a dam break on wet bottom, it seems possible to generate strong wave impacts in a short duration. This has to be verified experimentally specifically focusing on the measurements repeatability due to the obvious effect of the gate dynamics effect on the subsequent flow. When and if confirmed, this simple set-up could be used to validate numerical models without the need of a long propagation stage before impact.

Keywords: Dam break, wet bottom, wave impact, flip-through, Navier-Stokes model, Volume Of Fluid, impact pressure.

1. Introduction

Strong wave impacts may cause important damages on coastal or ocean structures such as breakwaters or marine renewable energy converters [16]. Additionally, for instance in ships carrying liquids in partially full tanks, violent sloshing phenomena can also lead to wave breaking susceptible to damage the membranes placed inside the tanks or endanger the stability of the vessel.

Email address: stephane.abadie@univ-pau.fr (S. Abadie)

The literature highlights four type of wave impacts (e.g., [24], [22]) depending on the position of breaking point with respect to the obstacle. In the case of a broken wave, a turbulent bore breaker with low vertical and uniform horizontal velocities is generated. In that case, the impact is dampened by the foam and as a result, pressure reaches relatively low values. When the breaking point is closer to the obstacle and in case of a plunging breaker, a volume of air can be entrapped between the wave and the wall. If this volume is significant, two pressure peaks can be observed. The first one corresponds to the crest impact on the wall while the second one is due to the compression of the air pocket and is applied on a larger zone for a longer duration. If the breaking point is located just before the wall, only a small air cushion is trapped and transformed into small bubbles after the impact. This kind of impact -referred to as "flip-through impact" when the air cavity is as small as possible - leads to the highest pressures. A very sharp single peak is observed sometimes followed by high frequency oscillations (due to the expansion and contraction of the small air pocket). The flip-through generates a very particular time history of pressures referred to as the "church roof profile" in Peregrine [48]. Finally, when the trough level reaches the theoretical impact point before the crest hits the wall, an upward deflected breaker is created. This kind of breaker leads to a sloshing impact for which two relatively small peaks are generally observed. They correspond to the first impact and then to the overturning of the upper part of the wave that was concave and becomes convex. Hull and Muller [25] and Scolan [52], both showed that a smooth transition between these four types of impacts could be obtained by increasing gradually the amplitude of the wave.

In the flip-through impact, the wave approaching the wall has a very steep (almost vertical) face. A flat impact could therefore be expected. Nevertheless, the wave trough is blocked by the wall and starts running-up on the wall which causes the focusing of the free surface at one point on the wall. This leads to the formation of a vertical jet with very high accelerations ($> 1000g$) and local pressures superior to $10\rho g(H + h)$ with h water depth and H wave height [48]. Experimental and numerical studies have been carried out in order to get a better understanding of the flip-through phenomenon. Lugni et al. [39] obtained waves impacts through the longitudinal forced motion (sway) of a prismatic tank (sloshing). Accelerations up to 1500 g were reported in this study. Hattori et al. [22], Hull and Muller [25], Hofland et al. [23], Kimmoun et al. [31], Brosset et al. [10], Mai et al. [40] generated violent impacts with focused waves in a flume. The latter are obtained by forcing several different waves of which the parameters are very finely tuned to exactly superimpose at the expected focal point.

Repeatability is a major concern when studying wave impact either experimentally or numerically, the peak pressure value being largely variable for the same impact conditions. This apparently chaotic behavior is due to the phenomenon, which mixes large scale processes (wave propagation, wave breaking) and very local water/air interface physics.

Related to the latter matter, Lubin et al. [37] for instance clearly showed the different instabilities which can lead to the atomization of the plunging jet in a breaking wave. As a result, it is very hard to ensure that the local wave shape and dynamics just before impact are exactly the same. For instance, in wave focusing, uncertainty may come from : the wave paddle motion, inaccuracies in the still water level that can strongly affect the focal point, small perturbations at the surface of the water due to the previous waves, instabilities of the wave crest (Kelvin-Helmoltz instability), etc. As a consequence, a very long and fine tuning of the parameters associated to a very high density of pressure sensors is necessary to capture the flip-through phenomenon.

Numerical studies were also conducted to study the flip-through impact. As a matter of fact, the first paper proving the existence of this particular impact is a numerical work [12]. The same author also showed that a parabolic shape of the free surface before impact is also a characteristics of the flip-though [13]. More recently, Bredmose et al. [9] compared experimental measurements of focused wave impacts and simulations based on a fully nonlinear potential-flow solver. Colicchio et al. [11] studied experimentally and numerically, with a SPH model solving the Navier-Stokes equations, the sloshing inside a tank subjected to horizontal oscillation. Scolan et al. [54] also compared numerical results obtained by means of a desingularized technique (potential flow solver) with the results of experimental sloshing of a prismatic basin. The latter study particularly underlined the importance of finding an easier way to simulate wave impacts compared to sloshing. Because of the complexity of the processes (focusing of waves and sloshing), the numerical models require a long time of computation before the actual impact often leading to difficulties in the results interpretation.

If we leave aside the problem of repeatability and now analyze the results of the studies, the main points of interest were the maximum impact peak pressures reached, the controversial vertical position of the maximum impact pressure and the presence of a vertical jet rising along the wall. Very high pressure peaks (i.e., in the range $10 - 100\rho gh$) were for instance obtained in Hattori et al. [22], Lugni et al. [39], Bredmose et al. [9], Hofland et al. [23].

The position of the maximum impact pressure on the wall remains a subject of debate. According to Hattori et al. [22], Minikin [43] and Goda [19], the pressure peak values are obtained at the still water level (SWL). Whereas Kirkgoz [32] and Allsop [4] observed peak values under the SWL. Hull and Muller [25] measured peak values at the SWL for the flip-through impacts and above the SWL for the cases with entrapped air. More recently, Hofland et al. [23] conducted a large scale experimental study and found the peak values to be reached above SWL for all impact cases. This characteristic of the impacts is still not clearly understood and needs further investigations. Another feature of the flip-through as described in Cooker and Peregrine [12], is the very fast jet rapidly rising along the wall just

before the crest hits the wall. Hull and Muller [25] added particle tracers to the flow but failed to prove the existence of the aforementioned jet. Peregrine [48]), Lugni et al. [39] and Scolan [52] obtained vertical accelerations of 1000g, 1500g and 1800g, respectively, the largest value likely being the 59000g reported in [13].

Many features of the wave impacts and in particular the flip-through impact need further investigation. Unfortunately, the lack of repeatability and the complexity of the experimental ways of generating impacts make it difficult to control accurately the wave shape. In this paper, we propose to use the dam break flow on wet bottom to generate wave impacts. This classical hydraulic flow allows to generates almost instantaneously a breaking wave [28] whose shape may be possible to control. Furthermore, by placing an obstacle at the right position relatively to the generated wave, one can hope to obtain an impact meeting for instance the conditions of the flip-through.

For a long period of time, studies mainly focused on the kinematic aspects of the dam-break flows (e.g., [55]). In the last 15 years, some works started including the dynamic aspects. Most of them consist in dry dam-break simulations and they are often limited to the validation of the numerical model used for one specific case of dam-break with no further intention of analyzing the dynamics of the impacts.

In the case of dry dam-break flow impacting an obstacle, limited values of peak pressures were usually measured : 4.5 ρgh [36], 1.35 ρgh [30], 3.25 ρgh [27], 2.7 ρgh [29], 2.3 ρgh [41], 2.4 ρgh [33] and 1.35 ρgh [45]. As mentioned before, one can expect pressures superior to 10 ρgh in the case of a flip-through impact. The magnitude of the aforementioned impacts stays therefore quite limited. Even so, the dry bed cases put in evidence some important characteristics of the dam-break that are also true in the case of the wet bottom.

First, the motion of the gate has a strong influence on the results. It is therefore necessary to take it into account in both, the numerical [29] and experimental [36] studies in order to obtain a good repeatability and a good agreement between the results. Then, by varying the upstream water depth or by moving the obstacle away from the gate, one can expect to observe interesting variations of the impact pressures on this obstacle. Aureli et al. [7] conducted several experiments in which the upstream depth varied from 7 to 13 cm in 5 mm steps. A quadratic relation between the impact peak force and the initial water depth in the tank could be highlighted. Issakhov et al. [26] moved the obstacle further from the gate and observed an increase of the impact pressure that was assumed to be caused by the increase of the flow velocity.

Very few studies specifically concentrate on the dynamics of wet dam-break induced wave impacts, and most of the time, the wet-bottom condition is a consequence of the remaining water in the flume after the previous test (insufficient drying time) or is due to leaks at the gate. More over, the impact studied is always the one of a turbulent bore

(e.g., [35]). Among those kind of studies, Al-Faesly et al. [3] for instance compared the pressures on a 1m high square column in the case of a dry bottom and a wet bottom dam-break with an upstream depth of 55 cm and a downstream depth of a few mm (2-3 mm). In the dry case, the maximal pressure, equal to 5 ρgh at 2 cm above the bottom of the flume was larger than in the wet case (i.e., 1.75 ρgh). Larger depths ratio (i.e., downstream to upstream depths) were used for instance in Arnason [6] or in Hartana and Murakami [21] but the maximal pressure generated on the obstacle is always less than 5 ρgh which is the typical values for bore impacts. More recently, Zuo et al. [59] employed a Large Eddy Simulation mesh-free incompressible model to study the impact of violent plunging breakers generated by large upstream to downstream water depth ratios. Relative pressure values $p/\rho gH$ (with H upstream water depth) of the order of 2 to 5 were obtained. Using a scaling with the downstream water depth, this would give values around 50 which is quite large. Nevertheless, only a few cases were investigated, the maximum pressure on the wall was not recorded, and all the impacts illustrated in the figures involved the formation of a pocket, which the monophasic incompressible model used could not properly describe.

The present paper proposes a first comprehensive study of the wave impacts generated in the wet dam break flow with a focus on the sloshing and flip-through impacts. In this work, the position of the obstacle with respect to the wave and the upstream water depth is varied to generate different impact types and obtain variable pressure values. This first study is purely numerical and will require further experimental validation to confirm the results obtained. Nevertheless, if slight variations in the results may be expected, we think that the overall conclusions of the paper will remain valid.

In section 2, the numerical model used and the set-up of the numerical experiment are presented. This set-up is based on Jánosi et al. [28], which serves as reference for the model validation. In section 3, the results of more than 500 hundred impact cases are presented and discussed in section 4. Finally, the main conclusions of this work are drawn in section 5.

2. Method

2.1. Model

The model used to perform this research is the multi-fluid Navier-Stokes Volume Of Fluid (VOF) model THETIS. It has been validated in numerous studies related to water waves [1, 38, 2, 46, 15, 17] and more specifically to wave impact in Mokrani and Abadie [45] and Martin-Medina et al. [42] .

The system of equations, also called one-fluid model, is composed of the incompressible Navier-Stokes (NS) equations (1) and an additional equation for the interface evolution (2) :

$$\begin{cases} \nabla.\mathbf{u} = 0 \\ \rho\left(\frac{\partial \mathbf{u}}{\partial t} + (\mathbf{u}.\nabla)\mathbf{u}\right) = \\ \rho\mathbf{g} - \nabla p + \nabla.\left[(\mu + \mu_t)(\nabla\mathbf{u} + \nabla^t\mathbf{u})\right] \end{cases} \quad (1)$$

$$\frac{\partial \chi}{\partial t} + \mathbf{u}.\nabla\chi = 0 \quad (2)$$

In which, ρ and μ, respectively density and viscosity of the fluid, are spatially varying variables and $\chi(x, y, t)$ is a phase characteristic function equal to 1 in water and 0 in air. In THETIS, a selective function has been implemented to check that the velocity field is locally turbulent. In this case, a Large Eddy Simulation model is turned on with a subgrid viscosity, μ_t, calculated with the Mixed Scale model as described in Lubin et al. [38].

The NS equations are discretized on a fixed Cartesian grid using a finite volume formulation. Following Patankar [47], the finite volumes formulation is solved using staggered mesh known as the Marker And Cells (MAC) method from Harlow and Welch [20]. For this reason, in THETIS the mesh is composed of two grids: the pressure grid and the velocity grid. The coupling between velocity and pressure is solved using the projection method [18].

Equation (2) is solved by introducing a color function F defined as the average of the phase characteristic function $\chi(x, y, t)$ over the mesh cell. With this definition, F indicates the volume fraction occupied by water in a mesh cell and the interface position is defined as the iso-line $F = 0.5$.

At the end of each time step, the local cell water volume fraction is used to recalculate local values of density and viscosity necessary to solve the NS equations. For cells containing a fraction of water and air, equivalent density and viscosity are calculated by interpolations based on the water and air fraction. The equivalent density is here obtained with a linear interpolation : $\rho_{eq} = \chi\rho_w + (1 - \chi)\rho_a$ (with subscript $_w$ for water and $_a$ for air), which exactly computes the amount of mass present in the cell, while the equivalent viscosity is computed with the following harmonic average : $\mu_{eq} = \frac{\mu_w\mu_a}{\chi\mu_w+(1-\chi)\mu_a}$, allowing to retrieve the right value of the viscosity in a simple shear flow [51].

Different VOF methods are implemented in the model THETIS to solve equation (2). The Piecewise Linear Interface Calculation (PLIC) method [58] is employed here with a correction step called SVOF-PLIC (S for Smooth). One of the great advantages of PLIC is to keep the discontinuous nature of the interface between water and air thanks to the Lagrangian character of the transport method. To ensure the stability of the PLIC method, a sufficient condition is that the segments are not advected over more than half of a cell size during a time step [1]. The SVOF-PLIC method, used in complement of PLIC, consists

in slightly smoothing the volume fraction function by introducing a controlled diffusion zone around the interface [49]. The color function includes a narrow diffusion zone that represents the interface more regularly. By this way, the discontinuities which may appear with the PLIC algorithm, and may sometimes lead to the computation divergence, are smeared and the interface is more stable while being a little less accurate. The model can then describe high interface distortions. Practically, the parameters and the number of internal iterations are adjusted to limit the interface fractioning while keeping an accurate description of the interface. The reader is referred to Pianet et al. [49] for a detailed description of the algorithm and a comparison of its efficiency with other classical interface tracking methods.

2.2. Numerical experiment

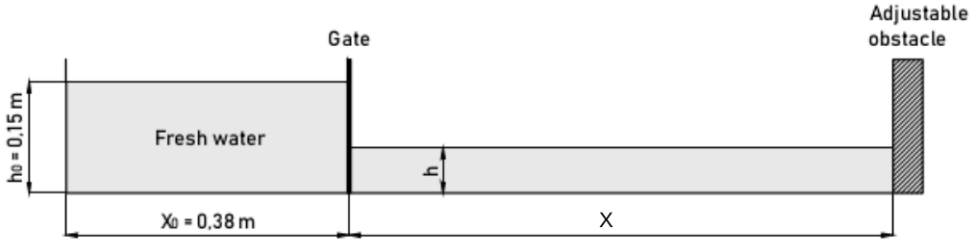

Figure 1: Sketch of the set-up studied and the associated parameters

In the wet dam breaking problem with an obstacle downstream (Figure 1, top panel), the problem parameters are : the upstream and downstream depths, respectively h_0 and h, the length of the upstream tank X_0 and the position of the obstacle X with respect to the gate position.

In our study, we considered the same general set-up as in Jánosi et al. [28] to benefit from their experimental results. h_0 is fixed to 0.15 m. Two cases were studied in Jánosi et al. [28], involving downstream water level h respectively equal to 0.018 and 0.038m. These two cases are used here as reference to validate the model without obstacle. For these two cases, the lateral downstream limit of the model is fixed at 2m from the gate. The mesh is irregular. In the horizontal direction, the grid step is exponentially decreasing from x=0 to x=0.38m (175 cells) down to 0.001m, equal to 0.001m from x=0.38m to x=0.78m (200 cells), and exponentially increasing, starting from 0.001m after x=0.78m (325 cells). In the vertical direction, the grid step is constant and equal to 0.0015m (200 cells between y=0 and y=0.3m). Free slip conditions are set to each boundary.

As already mentioned in Crespo et al. [14], and because during the experiment, the gate velocity was of the same order as the flow horizontal velocity, it was necessary to take into

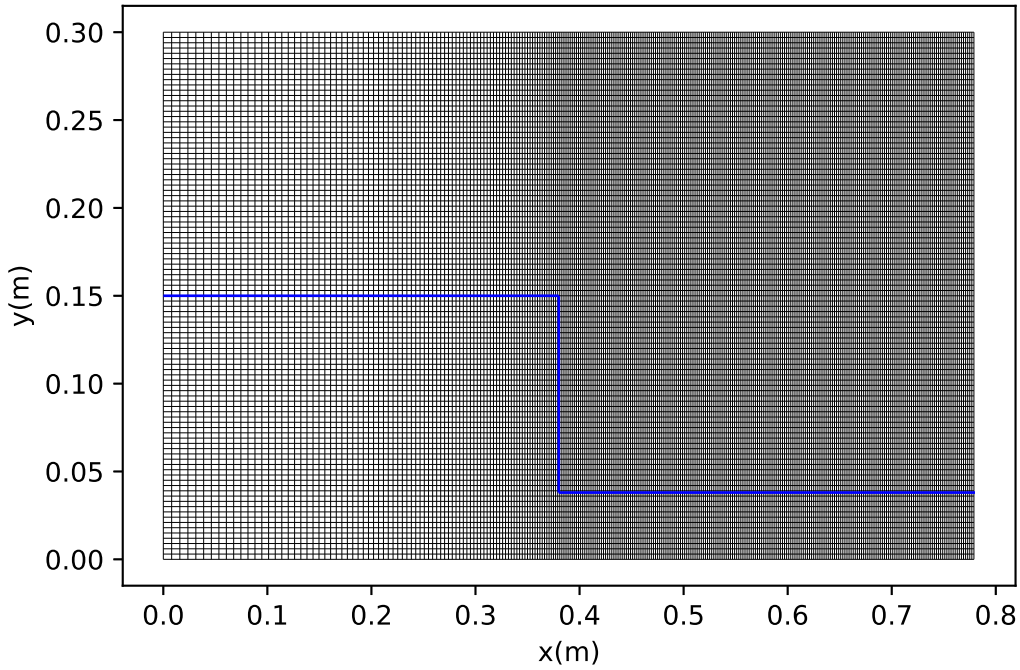

Figure 2: Representation of the mesh used for the numerical experiment here with $X = 0.40$ m, $h = 0.038$ m and position of water at t=0 in blue. Only one point out of four are plotted for the sake of readability.

account the kinematic of the dam gate to properly reproduce the experimental results. We tested a constant uplift velocity as well as a constantly accelerated uplift motion. The motion of the gate was stopped before it reached the free surface in order not to generate unwanted effects. By doing so, we avoided the water to be dragged with the gate and the generation of water droplets. For this reason, small rectangles can be observed in the next figures relatively to the type of impacts.

For the numerical experiment, most of the simulations were carried out for values of h between 0.018m and 0.038m (i.e., between the two values of the reference case for which the model was compared with the experiment) with a step for h of 1 mm. The numerical setting is the same as described previously, except that the downstream limit is fixed by the value of X. The horizontal mesh step is constant and equal to 1 mm after the gate (Figure 2) . For each value of the downstream depth h, cases were simulated starting from $X = 0.12$ m, with a step of 0.01m, until reaching the first entrapped air cases. Additional simulations were then carried out for values of h superior to 0.038 m in order to see if it was possible to reach higher pressures and peak pressures. As peak pressures started decreasing after h = 0.045 m, no further cases were simulated. Indeed, it is supposed that, with decreasing differences between h and h_0, the breaking point is more and more delayed, up to the point where it does not occur anymore. Therefore, the impact pressure is expected to decrease progressively as observed. On the lower end of the range, $h = 0.018$ m generates a breaking almost immediately after the gate release and the maximum impact pressure (i.e., varying X) was lower than for larger h. It was therefore considered as our lowest value. Conversely h_0 is not considered variable to keep the model close to the experimental set-up [28], to which it has been compared.

Overall, about 500 simulations were carried out. For each simulation, the maximum pressure and the position of this maximum in the vertical (i.e., z-axis) were calculated and recorded at each time step, one cell before the rightward domain boundary, which played the role of the obstacle. Additionally, to investigate the role of the interface shape before impact, a snapshot of the free surface was taken at this stage, providing the shape of the wave face and the associated local velocities (u the horizontal velocity and v the vertical velocity). This snapshot was taken as soon as the free surface increased for more than 20% of the initial water level, again one cell before the wall position. The magnitude of the velocity is then calculated from u and v and averaged over the free surface in a region close to the impact to get a characteristic impact velocity called V_{imp}. The other characteristic quantities are : the long wave celerity $c = \sqrt{gh}$ and a reference time $t_0 = h/c$.

3. Results

3.1. Validation of the model

The results of the numerical simulations have been compared with the snapshots obtained by Jánosi et al. [28](figure 3). As no pressure measurement was performed in the former reference, only wave shapes are compared. Nevertheless, according to Martin-Medina et al. [42], which used the same model THETIS, the correct reproduction of the shape and temporal evolution of the free surface guarantees similar impact pressure signals to be obtained. This is also a conclusion of the work performed in Mokrani and Abadie [45] using the same model.

Two cases were simulated with the downstream depth equal first to 18 mm and then to 38 mm. Experimental free surfaces have first been digitized in order to compare with the numerical simulation results. As our interest is focused on the wave just before it breaks, only the first four snapshots of each case were considered and digitized. The quality of the snapshots being quite low, it may be a source of imprecision in the following comparisons. This imprecision is of approximately 2mm when considering the height h of the downstream free surface on both pictures. These 2mm are responsible for a scale imprecision of more than 10% in the 18 mm case and 5% in the 38 mm case, which will affect the considered wave height and position of the wave front at a given time.

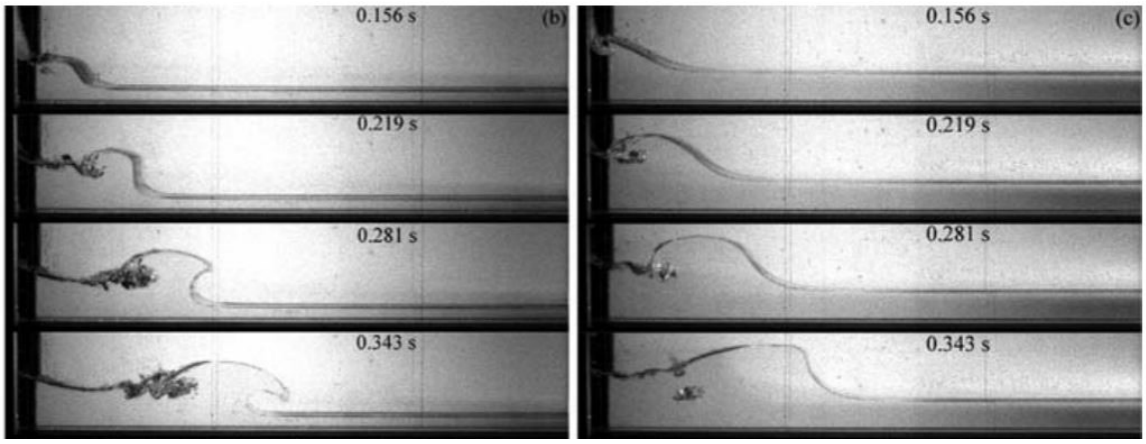

Figure 3: Snapshots from Jánosi et al. [28] with upstream water depth h_0=15 cm and downstream water depth, h=18 mm (left panel) and h=38 mm (right panel)

As can be seen on Figure 4, for a downstream depth of 18 mm, the model offers a good representation of the position of the wave front and height between 0.156 s and 0.343 s. One of the peculiarities of the wave, as generated in the experiment, is the leftwards breaking that can be observed in the two first snapshots. This feature is well represented

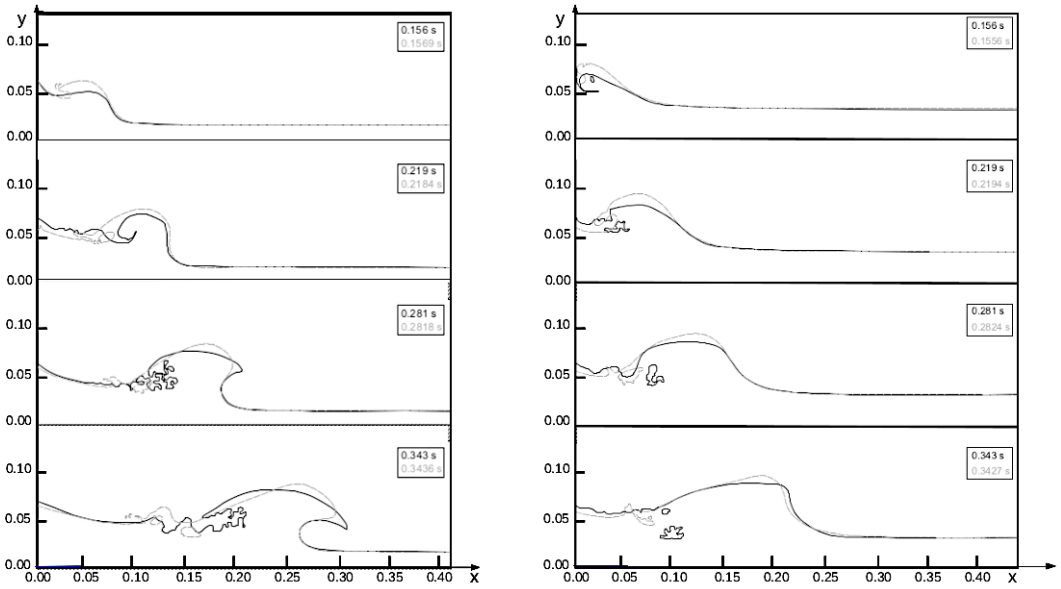

Figure 4: Comparison between experimental and numerical results for $h = 18mm$ (left) and $h = 38mm$ (right). Black curve : [28] grey curve : THETIS simulation.

by the numerical simulation. On the other hand, the model does not fit perfectly the wave breaking, especially the development of the breaking jet. Nevertheless, as the purpose of this work is focused on impacts without air entrapment, this late breaking process is not crucial. Nevertheless, it should be noted that the impact process being very sensitive to the slightest changes in wave geometry, the observable differences between experiment and simulation may generate non negligible differences on the peak pressures.

The results obtained for the 38 mm case are slightly better than those obtained for the 18 mm case. One explanation could be the larger scale of the case that reduces the effects of the imprecision of the picture.

A comparison between the results obtained with a 1.5 $m.s^{-1}$ constant velocity and with a uniformly accelerated gate (whose corresponding average velocity value is equal to 1.5 $m.s^{-1}$) has been performed (figure not shown here). The progression of the wave happens faster for the uniformly accelerated gate movement. The shape of the wave is also flattened in comparison with the constant velocity case. Finally, as in Crespo et al. [14], the best results were obtained with a constant velocity of $1.5m.s^{-1}$. This is the configuration used for the next numerical experiment.

A mesh study has also been conducted to see the effect of the resolution on the impact pressure estimated by the model (figure 5). The model set-up corresponds to the sketch

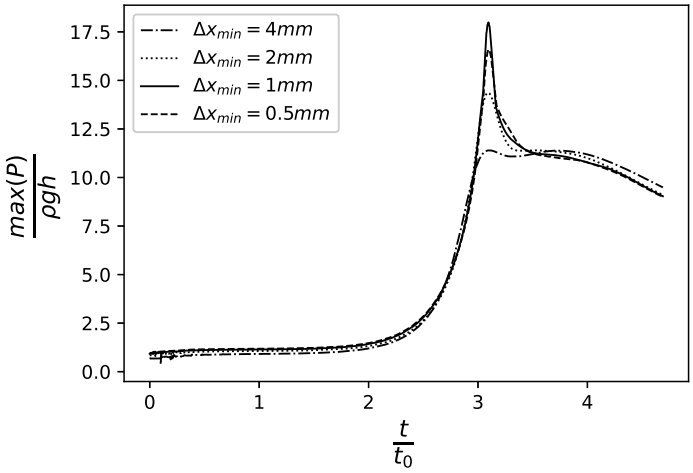

Figure 5: Maximum pressure on the wall for different mesh resolution, $h = 0.018$m and $X = 0.1$m.

of figure 1 leading to a very quick impact on the obstacle due to the limited downstream depth. The variable represented is the time variation of the maximum pressure on the wall which is of interest in this paper. Figure 5 shows that the peak first increase up to a maximum of about 17.5 with the resolution of 1mm and then decrease by 8% with the finest resolution of 0.5mm. The model convergence is therefore not perfectly achieved. This is not completely surprising owing to the combined difficulty of the gate/flow interaction with the inherent instability of the liquid impact problem. With the same model, Mokrani and Abadie [45] for instance showed the heavy resolution requirement to achieve convergence at the stagnation point in a dry dam break impact. Impact pressures are also shown to slightly vary with mesh resolution in the mesh-free simulations presented in Zuo et al. [59]. Methods used to track the interface are also susceptible to generates discrepancies in the peak pressure computed [34]. Furthermore, convergence is more easily achieved on the pressure impulse than on the pressure peak [5, 44]. Therefore, the choice of the 1mm resolution for the numerical experiment is a compromise between accuracy and CPU constraints. Nevertheless, due to the aforementioned numerical limitations, the individual pressure peak values computed may not be completely accurate while the relative trend is expected to be more trustful.

3.2. Numerical experiment

Several types of impacts were obtained depending on the position of the obstacle (X) with respect with the breaking point location (itself depending on the water depth h). Two

processes happen simultaneously. The progression of the wave forces the wave trough to run-up quickly along the wall while the wave crest moves forward more slowly. The time history of these two phenomenons and the fact that they coincide or not is responsible for the type of impact generated on the obstacle. Hence, four types of impacts were observed : sloshing impacts (Figure 6), flip-through impacts (Figure 7), air pocket impacts (Figure 8), broken wave aerated impacts (Figure 9). The flip through impact, which is the limiting case after which air starts to be entrapped, is characterized by the birth of a small vertical jet (not visible on the figure) associated to very large accelerations. As mentioned before, the presence of small rectangles in the figures is due to the fact that the motion of the gate is stopped before it interferes with the free surface.

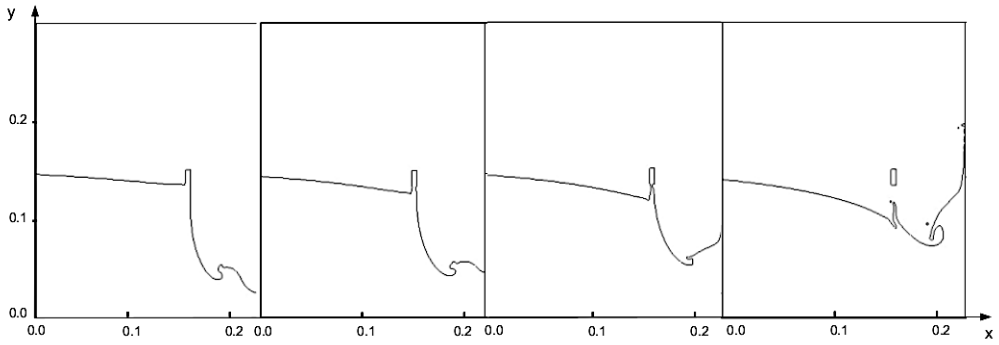

Figure 6: Sloshing impacts obtained for $h = 18mm$ and $X = 0.07m$ at $t = 0.12, 0.16, 0.25$ and $0.40s$.

The two cases studied in Jánosi et al. [28] are described in terms of kinematic and dynamic of the impacts generated depending on the position of the obstacle (Figures 10 and 11). The bottom panel shows the obstacle position for which, the first pressure peak appears on the wall. For instance for the case h=18mm, the critical position is X=0.075 m. Before the latter, the largest pressure is on the bottom ($z_{p_{max}}$=0) as pressure is purely hydrostatic. After this limit, a larger pressure peak appears on the wall (i.e., no longer on the bottom part). Up to the limit case of the flip-through (marked by the $\triangledown$ symbol), we refer to these kinds of impacts as sloshing impacts (marked by the + symbol). Right after the flip-through case, air entrapment starts to be observed. Even though the incompressible code is not supposed to represent properly the actual process when air entrapment occurs, results are plotted to give some information on the evolution of the parameters when passing through the flip-through limit. For the two downstream water heights studied (i.e., 18mm and 38mm), and whatever the impact type, the pressure peak occurs at a very stable relative altitude $z_{p_{max}}/h \approx 2.5 - 2.75$. The value of $\frac{V_{imp}}{c}$ for the low water depth case, linearly increases from about 1.3 when X is the smallest to about 1.75 after the

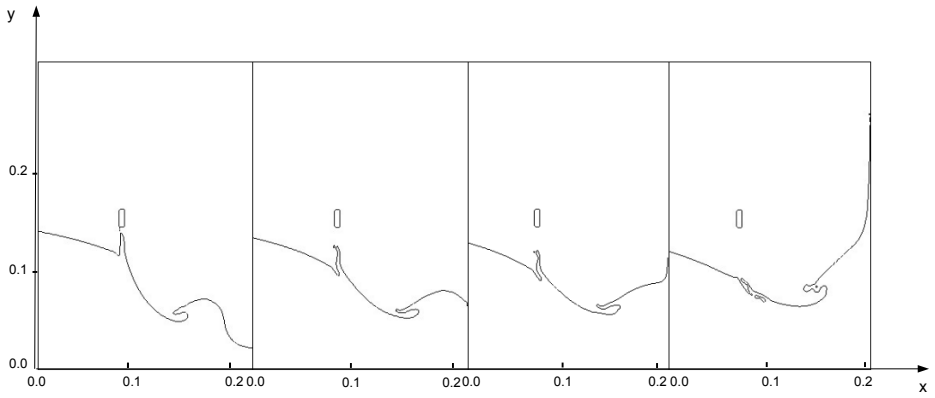

Figure 7: Flip-through impacts obtained for $h = 18mm$ and $X = 0.119m$ at $t = 0.22, 0.31, 0.38$ and $0.61s$

flip-through position. In the larger depth case, it is very stable around 1. It is likely that the more distant obstacle, in the larger depth case, allows for a stabilization of the wave front velocity whereas in the low depth case, the position of the obstacle is closer to the gate and therefore the flow velocity is still rapidly evolving. As for the pressure peak, it is shown to gradually increase in absolute value as well as in relative value (i.e., scaled by dynamic pressure) in both cases as soon as the pressure maximum is no longer hydrostatic. Note that air entrapment does not drive any change in this evolution (the curve being perfectly continuous). The flip-through impact obtained for a downstream depth of 18mm generates a peak pressure of $6.185kPa$ for $X = 0.119m$ while the 38mm case gives rise to a $10.36kPa$ pressure peak when $X = 0.32m$. Interestingly, similar peak values are obtained when the pressure is scaled by the initial hydrostatic pressure (35 against 27.7 for h=18 and 38 mm respectively) whereas a larger difference is obtained with dynamic pressure as reference (12.5 against 28).

Figure 12 shows the evolution of pressure at z_{pmax} with time for simulations involving different values of X. These simulations can be separated into two groups. The first one, represented with black dotted lines, corresponds to cases where the pressure maximum is reached at the bottom of the water (i.e., between $X = 0.02m$ and $X = 0.074m$ for $h = 18mm$ and between $X = 0.12m$ and $0.22m$ for $h = 38mm$). In those cases, the time evolution of pressure is relatively slow and the pressure maximum is equal to the hydrostatic pressure value corresponding to the wave run-up on the wall. The second group, plotted with

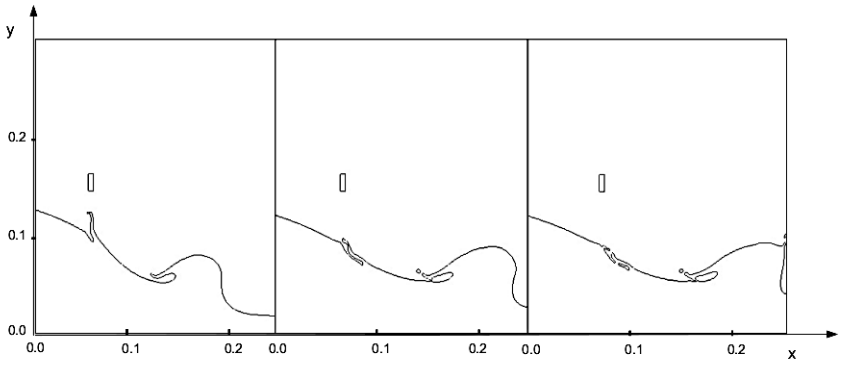

Figure 8: Impacts with entrapped air obtained for $h = 18mm$ and $X = 0.17m$ at $t = 0.28, 0.365$ and $0.435s$

continuous lines, corresponds to sloshing impacts. They are obtained for positions of the right wall between $X = 0.075m$ and $X = 0.118m$ for $h = 18mm$ and between $X = 0.23m$ and $0.32m$ for $h = 38mm$. Here, the maximum of pressure is not reached at the bottom of the water but at a higher point on the obstacle. The pressure peaks are short (approximately $0.01s$) and their amplitude gets bigger and bigger as X increases. In the two cases plotted, the highest peaks are obtained for the flip-through impacts represented with red lines (further cases involving air entrapment are not considered in that plot).

The results obtained for all the simulations performed in this study are summarized in contour plots (figures 13, 14, 15, 16 and 17).

Figure 13 shows the distribution of the maximum pressure in the $X - h$ domain. Two grey lines approximately discriminates the three observed regimes (i.e., hydrostatic, sloshing and aerated). In the hydrostatic area, the pressure maximum is generated at the bottom by the water local elevation and its value is quite uniform in this domain. The gradient is much larger in the sloshing regime where an actual peak is observed in the pressure time signal. The flip-through occurs around the second grey line, crossing higher pressure contours, and which equation is : $\frac{h}{h_0} = 0.103\frac{X}{h_0} + 0.032$. The area corresponding to aerated impacts (broken waves) or impacts with entrapped air (below the grey line representing the air entrapment limit) are the ones that engender the highest pressures in this study, but these cases have to be considered with caution as compressibility is not considered in the model.

In Figure 14, the maximum pressure is divided by ρgh. In the hydrostatic area, the contours give an idea of the run-up generated by the impact on the vertical wall. In the sloshing area, the maximum value (i.e., about 35) of this non-dimensionalized pressure is obtained for the smaller scale case with $h = 0.018m$ and $X = 0.119m$. Along the limit of

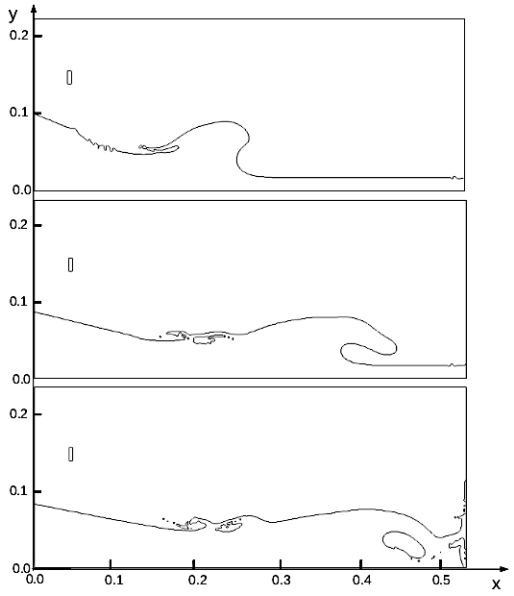

Figure 9: Impact obtained after the wave has totally broken for $h = 18mm$ and $X = 0.47m$ at $t = 0.3639$ and $0.3861s$

air entrapment (i.e., flip-through cases), $P/\rho gh$ then decreases gradually with increasing h.

The maximum impact velocities V_{imp}, larger than $1.68\sqrt{gh}$, appears for X between 0.12 and 0.16 m and h lower than 0.19 m (Figure 15), namely for relatively small values of h and X). The relative impact velocity then decreases concentrically and regularly with increasing X and h. For a given h and starting from the lowest X value, the impact velocity first increases toward a maximum value. After reaching its maximum, for cases with $h < 0.037$, the impact velocity then decreases when the obstacle is moved further away and air starts to be entrapped. For larger h, the impact velocity is more or less constant after the first observed increase. Nevertheless, for all the cases, the impact velocity decreases beyond the air entrapment limit.

When scaled relatively to the dynamic pressure, the non-dimensional pressure is the highest for the cases involving large values of X and h (Figure 16), contrasting to the behaviour observed in Figure 14. Between the two grey lines, the flip-through impacts generate the highest pressures, with maximum relative pressure starting from slightly less than $15\rho {V_{imp}}^2$ (bottom part of the grey line delineating air entrapment) to approximately $30\rho {V_{imp}}^2$ (top part of the same grey line). For a given h, peak pressures then decrease quite linearly as sloshing impacts are considered (i.e., for X decreasing). On the left of the hydrostatic limit (top grey line), the relative pressure is almost constant (around 6) reflecting the weak spatial variation of V_{imp} and P in this area.

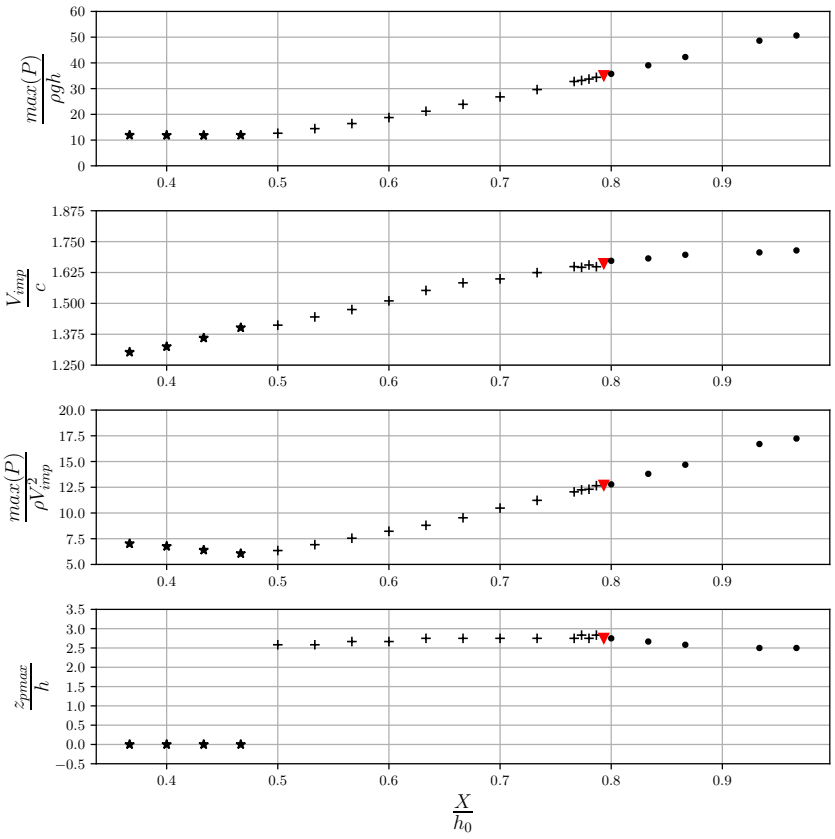

Figure 10: From top to bottom panel : maximum pressure recorded on the wall scaled by hydrostatic pressure, non dimensional impact velocity, maximum pressure recorded on the wall scaled by dynamic pressure and non dimensional height of pressure maximum versus X/h_0 for $h = 18mm$. Symbols used : $*$ for hydrostatic process (no pressure peak), + for sloshing, $\triangledown$ for flip-through and $\bullet$ for air entrapment.

Figure 17 shows the heights where the impact peak pressures are generated. Peak pressures appear at heights between 2 and 3 times the water depth h for the sloshing impacts, the largest values being associated to low water depths and the smallest to high water depths. Close to the flip-through impact limit, the values of z_{pmax}/h are in the range of 2.3 - 2.8 and start decreasing when getting closer to the grey line. Therefore, the height of maximum pressure seems to be a good indicator of the parameters for which a flip-through impact occurs.

Finally, accelerations of the free surface at the wall has been calculated for several cases along the grey line approaching the flip-through limit (Figure 18). To perform this

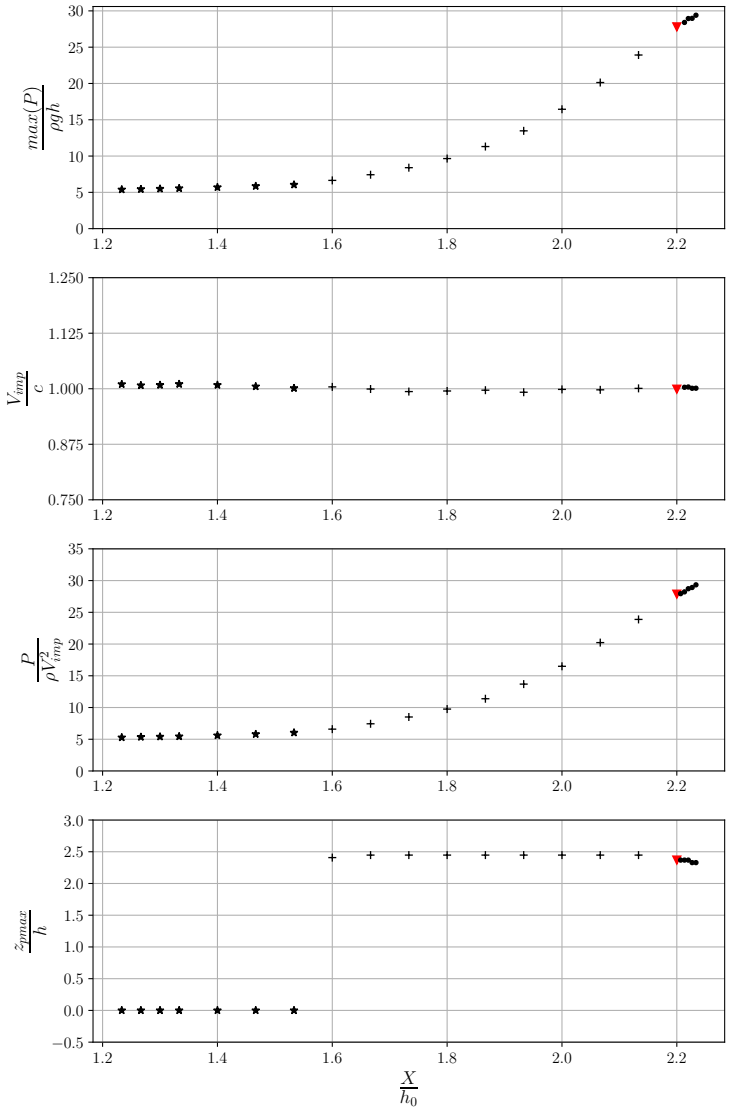

Figure 11: Same legend as previous figure with $h = 38mm$

computation, the free surface elevation next to the wall is first recorded and an exponential law fitted up to the visible inflection point after which acceleration decreases (i.e., black curves on Figure 18 left). The exponential is then analytically derived twice to retrieve the acceleration value (Figure 18 right). The maximum accelerations found with this method are between 76 and 142g, the largest value approximately corresponding to the area (e.g.,

Figure 14) where the pressure peak is the largest.

4. Discussion

In this work, we numerically studied wave impacts generated in the wet dam break flow. Based on two parameters, about five hundred distinct cases were obtained and resulted in different peak pressures on the obstacle. All the impacts can be grouped in four types : sloshing impacts, flip-through impacts, air pocket impacts and broken waves impacts.

These four types of impacts have already been described in the literature before but their modes of generation were different and generally required a longer time span from wave generation to impact. This longer duration adds to the inherent difficulty of the phenomenon, for instance in terms of repeatibility. Brosset et al. [10] stresses the problem of repeatibility when trying to reproduce a flip-through impact with wave focusing. In this study, the flip-through was obtained only once among 140 tests and for this, preliminary tests were first performed on a smaller tank to have a better control over the repeatability of the flow. In Hofland et al. [23], also based on wave focusing, among the 137 measured impacts, only 8 were identified as actual flip-through impacts. As underlined in this article, for a same configuration (same depth and focal distance) only approximately one test out of 10 gave rise to a flip-through impact. Sloshing in a prismatic tank has also be used to generate violent impacts (e.g., [39]) and the problem of repeatability arises generally in that case too. Impacts generated by wave shoaling in a flume (e.g., [31]) can also be affected by a lack of repeatability due to the poor repeatability of the wave maker itself and the difficulty to control the water depth in the wave flume. A long generation mode also leads to very large data set due to the very high sampling rate required to capture the impact phenomenon. It is also a supplementary difficulty for numerical simulation. Indeed, in order to predict the proper impact dynamic, one has to reproduce very accurately the wave shape just before impact. This implies perfectly solving the generation and propagation stage, which may already be a challenge for the models. This usually requires heavy model coupling techniques to be employed [53]. In the present paper, wave impact is generated very quickly after removing the reservoir gate. The wave is created instantaneously by the interaction of the water volume released with the downstream fluid. It is a very simple configuration which can be easily used in any laboratory. Note that repeatability has still to be checked experimentally. For this, the gate lift control will probably be of the utmost importance.

In figure 12, in both reference cases, a very sharp and high peak of pressure was observed close to the air entrapment limit. This shape, often referred to as a ”church roof shape” [48], is a consequence of the large vertical acceleration due to the presence of the

obstacle. In the critical flip-through cases (e.g., Figure 7), this acceleration reaches a maximum due to the existence of a more or less ideal focal point toward which, a large amount of the fluid particles converges [39]. In the present study, the vertical accelerations of the free surface close to the obstacle are approximately in the range $50 - 150g$ (Figure 18). These large values are nevertheless lower than the extreme values usually reported in the literature (see section 1) likely due to the reduced dimension of the set-up studied. The maximum pressures obtained with this dam break configuration are of the order of $10kPa$ and relatively to the hydrostatic pressure, of the order of 30. This is clearly in the range 10-100 ρgh associated to the strongest impacts reported in the literature [39] and one order of magnitude larger than the values so far reported in the impacts generated in dam break flows. Along the grey line delineating sloshing and aerated impacts (Figure 13), given by the equation $\frac{h}{h_0} = 0.103\frac{X}{h_0} + 0.032$, starting from the lower water depths, the peak pressure first increases to reach a maximum around $h \approx 0.036$ (or $h/h_0 \approx 0.24$) and then decreases. The existence of this maximum was expected. Indeed, one may expect the flow to reach the ideal condition to generate the highest pressure peak between the very low downstream water depths, for which the wave shape may not be optimal and the high downstream water depths, which may attenuate the wave dynamic and even prevent its breaking for the largest values. Therefore, critical impacts (i.e., flip-through) exists for each h but there are some slight variations among them, dependent on the wave shape and the local velocity field generated.

When scaled relatively to the dynamic pressure, the maximal values are again around 30 (Figure 16), which also corresponds to large peak pressure values reported in the liquid impact literature [57]. Note that the variable $\mathrm{Max}(P)/\rho V_{imp}^2$ is more relevant than $\mathrm{Max}(P)/\rho gh$ to characterize the efficiency of the impact process to transform the wave momentum into a pressure peak. As mentioned in Mokrani and Abadie [45] and Martin-Medina et al. [42], this efficiency strongly depends on the flow horizontal velocity, hence the introduction of V_{imp}, but also, and to a large extent, to the water-air interface local angle. Figure 16 shows that this efficiency is maximum approximately where pressure is also maximum.

In the present work, the pressure peaks associated to sloshing impacts are located significantly above the water height h. For the flip-through impacts, this height is equal to $2.3h$ to $2.8h$. This result stresses the difference between regular (or irregular) wave impact and the present case. In the former cases, the free surface involves a through and a crest and the pressure peak, generated by the breaking wave impact, is, as already pointed out in the introduction, usually located near the average water level [19]. In the present study, the process significantly differs due to the water volume added in the domain after $t = 0$ and therefore, results are not comparable. Similarly, the waves dynamics also differ. A regular wave is free and the breaking is generated most of the time by the water depth

reduction. In the present case, the wave is forced by the pressure gradient due to the dam break. Nevertheless, to that respect, Figure 15 shows that, except for very small h values, the flow velocity associated to the breaking wave is close to the free shallow water wave celerity, which is what may be expected for a free wave breaking.

The main limitation of this study is the purely numerical approach proposed. Regarding this concern, the model has been validated in former studies related to wave impacts [45, 42]. From these studies, it is known that the pressure field accuracy depends on the velocity and local interface proper resolution at impact. Here, even if this model has been carefully compared to experimental results [28], uncertainties remain. The gate velocity law may not be exactly the same as in the experiment. It is not possible to verify this point as no reference was made in the associated article on that aspect. There is also a slight shift between the experimental [28] and simulated free surfaces. As the pictures quality is quite low, it is hard to know which part to attribute to the digitization process or to the actual weaknesses of the model. We also showed that the pressure peak is particularly sensitive to the mesh resolution (Figure 5).

Finally, the choice of an incompressible model to study water wave impacts may be argued. It is indeed well known that compressible effects plays a role in this phenomenon, especially when air is entrapped. In this case, the air pocket may oscillate and this translates to the pressure on the wall [8]. Additionally, the presence of air bubbles in water may lead to water compressibility allowing the generation of pressure waves [50]. Those effects are susceptible to really appear if the wave impact occurs after the breaking point. If this is not the case, then the flow stays mainly incompressible during the impact process. Very large pressure can anyway be generated [56]. From a numerical point of view, it is difficult to study incompressible flows with a compressible model and vice-versa. The point of view defended in this paper is to concentrate first on the incompressible part of the problem before focusing later on the compressible aspects. Therefore, the results given after the flip-through limit, where air is supposed to be entrapped, should obviously be interpreted with the highest caution. Those limitations given, the numerical results should not depart too much from the real phenomenon and provide a valuable guidance for a further and necessary experimental confirmation.

5. Conclusions

In this paper, a Navier-Stokes VOF model was used to study the wave impacts generated in a wet dam break flow when varying the position of the downstream wall and water depth. The following conclusions can be drawn from this work :

- first, to reproduce accurately the shape of the wave observed in our experimental reference [28], a gate motion had to be taken into account in the simulations,

- in the range of parameters tested, for a downstream water depth h and increasing progressively the impacted wall position, the following phenomena are observed : hydrostatic run-up, sloshing impacts, flip-trough impacts, air-pocket impacts and broken wave interaction with the wall,

- flip-trough impacts are defined as the limit case of the sloshing impacts just before air entrapment could be observed. For the wet dam break flow, we show that this condition is met for $\frac{h}{h_0} \approx 0.103\frac{X}{h_0} + 0.032$. Along this line, the free surface vertical acceleration is in the range 50 to $150g$. We also showed that among all the possible flip-through impacts, there is one optimum generating a pressure peak larger that the others,

- compared to impact pressures recorded or simulated with a dam break flow in previous studies (except the recent work of Zuo et al. [59] already discussed), the present numerical work reached values one order of magnitude larger (i.e. $P_{max} \approx 35\rho gh$ or $P_{max} \approx 30\rho V_{imp}^2$). Those values are in line with usual extreme pressures reported in wave impacts [39],

Therefore, wet dam break flow may be used to quickly generate a given wave impact adjusting the parameter of the experiment. Nevertheless, as this study is purely numerical, an experimental confirmation would be the logical perspective of this work. The future experiments should focus on measurements repeatability, as slight changes in the gate dynamics could modify the subsequent flow enough to make the pressure peaks unrepeatable. Additionally, by modifying the equilibrium between the different forces at stake, the experiment scale could also play a role on the shape of the wave for a given set of parameters and completely change the previous conclusions. Finally, the compressible impacts when air is entrapped have still to be tackle numerically. This is also a perspective of the present work.

6. Acknowledgments

This research was carried out under the framework of the joint laboratory KOSTARISK and within the HPC Waves chair. KOSTARISK is co-funded by E2S UPPA (ANR-16-IDEX-0002), the AZTI Foundation and the center Rivages Pro Tech of SUEZ. The chair HPC-Waves chair is financed by E2S UPPA, the Communauté d'Agglomération Pays Basque (CAPB), and the Communauté Région Nouvelle Aquitaine (CRNA). L.E. Dumergue acknowledges financial support from Ecole Normale Supérieure Paris Saclay for her PhD fellowship.

References

[1] Abadie, S., Caltagirone, J., and Watremez, P. (1998). Splash-up generation in a plunging breaker. *C.R.A.S. - mechanics*, Serie II.b:553–559.

[2] Abadie, S., Morichon, D., Grilli, S., and Glockner, S. (2010). Numerical simulation of waves generated by landslides using a multiple-fluid navier–stokes model. *Coastal engineering*, 57(9):779–794.

[3] Al-Faesly, T., Palermo, D., Nistor, I., and Cornett, A. (2012). Experimental modeling of extreme hydrodynamic forces on structural models. *International Journal of Protective Structures*, 3(4):477–505.

[4] Allsop, N. (1999). New design methods for wave loading on vertical breakwaters under pulsating and impact conditions. *Coastal structures*, 99.

[5] Arai, M., Cheng, L.-Y., Kumano, A., and Miyamoto, T. (2002). A technique for stable numerical computation of hydrodynamic impact pressure in sloshing simulation. *Journal of the society of naval architects of Japan*, 2002(191):299–307.

[6] Arnason, H. (2005). *Interactions between an incident bore and a free-standing coastal structure*. University of Washington.

[7] Aureli, F., Dazzi, S., Maranzoni, A., Mignosa, P., and Vacondio, R. (2015). Experimental and numerical evaluation of the force due to the impact of a dam-break wave on a structure. *Advances in Water Resources*, 76:29–42.

[8] Bagnold, R. (1939). Interim report on wave-pressure research.(includes plates and photographs). *Journal of the Institution of Civil Engineers*, 12(7):202–226.

[9] Bredmose, H., Raby, A., Jayaratne, R., and Bullock, G. (2010). The ideal flip-through impact - experimental and numerical investigations. *Journal of Engineering Mathematics*, 67:115–136.

[10] Brosset, L., Lafeber, W., Bogaert, H., Marhem, M., carden, P., and Maguire, J. (2011). A mark iii panel subjected to a flip-though wave impact : Results from the sloshel project. *Proceeding of the Twenty-first (2011) Internationnal Offshore and Polar Engineering Conference*, pages 84–96.

[11] Colicchio, G., Colagrossi, A., and Lugni, C. (2007). Challenges in the numerical investigation of the flip-through. In *IXth International Conference on Numerical Ship Hydrodynamics*.

[12] Cooker, M. and Peregrine, D. (1992). Wave impact pressure and its effect upon bodies lying on the sea. *Coastal Engineering*, 18:205–229.

[13] Cooker, M. J. (2010). The flip-through of a plane inviscid jet with a free surface. *Journal of Engineering Mathematics*, 67(1):137–152.

[14] Crespo, A., Gómez-Gesteira, M., and Dalrymple, R. A. (2008). Modeling dam break behavior over a wet bed by a sph technique. *Journal of waterway, port, coastal, and ocean engineering*, 134(6):313–320.

[15] Desombre, J., Morichon, D., and Mory, M. (2013). Rans v2–f simulation of a swash event: Detailed flow structure. *Coastal Engineering*, 71:1–12.

[16] Dias, F. and Ghidaglia, J.-M. (2018). Slamming: Recent progress in the evaluation of impact pressures. *Annual Review of Fluid Mechanics*, 50:243–273.

[17] Ducassou, B., Nuñez, J., Cruchaga, M., and Abadie, S. (2017). A fictitious domain approach based on a viscosity penalty method to simulate wave/structure interaction. *Journal of Hydraulic Research*, pages 1–16.

[18] Goda, K. (1979). A multistep technique with implicit difference schemes for calculating two-or three-dimensional cavity flows. *Journal of Computational Physics*, 30(1):76–95.

[19] Goda, Y. (1975). New wave pressure formulae for composite breakwaters. *Coastal Engineering*, 1974:1702–1720.

[20] Harlow, F. H. and Welch, J. E. (1965). Numerical calculation of time-dependent viscous incompressible flow of fluid with free surface. *The physics of fluids*, 8(12):2182–2189.

[21] Hartana and Murakami, K. (2015). Numerical and experimental simulation of two-phase tsunami flow through buildings with openings. *Journal of Earthquake and Tsunami*, 9(03):1550007.

[22] Hattori, M., Arami, A., and Yui, T. (1994). Wave impact pressure on vertical walls under breaking waves of various types. *Coastal Engineering*, 22:79–114.

[23] Hofland, B., Kaminski, M., and Wolters, G. (2011). Large scale wave impacts on a vertical wall. *Coastal Engineering Proceedings*, 1(32):15.

[24] H.Oumeraci, Klammer, P., and Partencsky, H. (1993). Classification of breaking wave loads on vertical structures. *Journal of WaterWay, Port Coastal and Ocean Engineering*, 119:381–398.

[25] Hull, P. and Muller, G. (2002). An investigation of breaker heights, shapes and pressures. *Ocean Engineering*, 29:59–79.

[26] Issakhov, A., Zhandaulet, Y., and Nogaeva, A. (2018). Numerical simulation of dam break flow for various forms of the obstacle by vof method. *International Journal of Multiphase Flow*, 109:191–206.

[27] Jančík, P. and Hyhlík, T. (2019). Pressure evaluation during dam break using weakly compressible sph. In *EPJ Web of Conferences*, volume 213, page 02030. EDP Sciences.

[28] Jánosi, I. M., Jan, D., Szabó, K. G., and Tél, T. (2004). Turbulent drag reduction in dam-break flows. *Experiments in Fluids*, 37(2):219–229.

[29] Kamra, M. M., Al Salami, J., Sueyoshi, M., and Hu, C. (2019). Experimental study of the interaction of dambreak with a vertical cylinder. *Journal of Fluids and Structures*, 86:185–199.

[30] Khayyer, A. and Gotoh, H. (2009). Modified moving particle semi-implicit methods for the prediction of 2d wave impact pressure. *Coastal Engineering*, 56(4):419–440.

[31] Kimmoun, O., Ratouis, A., and Brosset, L. (2010). Sloshing and scaling : Experimental study in a wave canal at two different scales. *Proc. 20th Int. Offs. and Polar Engineering Conference*.

[32] Kirkgoz, M. (1982). Shock pressure of breaking waves on vertical walls. *Journal of waterway, port, coastal, and ocean engineering*, 108:81–95.

[33] Kleefsman, K., Fekken, G., Veldman, A., Iwanowski, B., and Buchner, B. (2005). A volume-of-fluid based simulation method for wave impact problems. *Journal of computational physics*, 206(1):363–393.

[34] Li, Y. and Yu, C. (2019). Research on dam-break flow induced front wave impacting a vertical wall based on the clsvof and level set methods. *Ocean Engineering*, 178:442–462.

[35] Liu, J., Hayatdavoodi, M., and Ertekin, R. C. (2019). Bore pressure on horizontal and vertical surfaces. In *ASME 2019 38th International Conference on Ocean, Offshore and Arctic Engineering*. American Society of Mechanical Engineers Digital Collection.

[36] Lobovskỳ, L., Botia-Vera, E., Castellana, F., Mas-Soler, J., and Souto-Iglesias, A. (2014). Experimental investigation of dynamic pressure loads during dam break. *Journal of Fluids and Structures*, 48:407–434.

[37] Lubin, P., Kimmoun, O., Véron, F., and Glockner, S. (2019). Discussion on instabilities in breaking waves: Vortices, air-entrainment and droplet generation. *European Journal of Mechanics-B/Fluids*, 73:144–156.

[38] Lubin, P., Vincent, S., Abadie, S., and Caltagirone, J. (2006). Three dimensional large eddy simulation of air entrainment under plunging breaking waves. *Coastal engineering*, 53:631–655.

[39] Lugni, C., Brocchini, M., and Faltinsen, O. (2006). Wave impact loads : The role of the flip-through. *Physics of Fluids*, 18:122101–122118.

[40] Mai, T., Raby, A., and Mai, C. (2019). Aeration effects on water structure impacts : Part 2 – wave impacts on a truncated vertical wall. *Ocean Engineering*, 186.

[41] Marrone, S., Antuono, M., Colagrossi, A., Colicchio, G., Le Touzé, D., and Graziani, G. (2011). δ-sph model for simulating violent impact flows. *Computer Methods in Applied Mechanics and Engineering*, 200(13-16):1526–1542.

[42] Martin-Medina, M., Abadie, S., Mokrani, C., and Morichon, D. (2018). Numerical simulation of flip-through impacts of variable steepness on a vertical breakwater. *Applied Ocean Research*, 75:117–131.

[43] Minikin, R. (1963). Winds, waves, and maritime structures : studies in harbour making and in the protection of coasts. *Griffin*.

[44] Mokrani, C. (2012). *Impacts de vagues déferlantes sur un obstacle vertical. Modele théorique et calcul numérique des pics de pression*. PhD thesis, Pau.

[45] Mokrani, C. and Abadie, S. (2016). Conditions for peak pressure stability in vof simulations of dam break flow impact. *Journal of Fluids and Structures*, 62:86–103.

[46] Mory, M., Abadie, S., Mauriet, S., and Lubin, P. (2011). Run-up flow of a collapsing bore over a beach. *European Journal of Mechanics-B/Fluids*, 30(6):565–576.

[47] Patankar, S. (1990). Numerical heat transfert and fluid flow. *Hemisphere publishing Corporation, New york*.

[48] Peregrine, D. (2003). Water-wave impact on walls. *Annual Review Fluid Mechanics*, 35:23–43.

[49] Pianet, G., Vincent, S., Leboi, J., Caltagirone, J., and Anderhuber, M. (2010). Simulating compressible gas bubbles with a smooth volume tracking. *International Journal of Multiphase Flow*, 36:273–283.

[50] Plumerault, L.-R., Astruc, D., and Maron, P. (2012). The influence of air on the impact of a plunging breaking wave on a vertical wall using a multifluid model. *Coastal engineering*, 62:62–74.

[51] Ritz, J.-B. (1997). *Modélisation numérique des écoulements fluide-particules: définition d'un modèle de simulation directe, application à la sédimentation*. PhD thesis, Bordeaux 1.

[52] Scolan, Y.-M. (2010). Some aspects of the flip-though phenomenon : A numerical study based on the desingularized technique. *Journal of Fluids and Structures*, 26:918–953.

[53] Scolan, Y.-M., Brosset, L., et al. (2016). Numerical simulation of highly nonlinear sloshing in a tank due to forced motion. In *The 26th International Ocean and Polar Engineering Conference*. International Society of Offshore and Polar Engineers.

[54] Scolan, Y.-M., Lauzon, J. D., and O.Kimmoun (2010). The flip-through : fluid kinematics and hydrodynamic loads. In *XXII Journée de l'Hydrodynamique, France, Nantes, 17-19 novembre*.

[55] Stoker, J. (1957). Water waves, pure and applied mathematics.

[56] Wagner, H. (1932). Über stoß-und gleitvorgänge an der oberfläche von flüssigkeiten. *ZAMM-Journal of Applied Mathematics and Mechanics/Zeitschrift für Angewandte Mathematik und Mechanik*, 12(4):193–215.

[57] Wu, G. (2007). Fluid impact on a solid boundary. *Journal of fluids and structures*, 23(5):755–765.

[58] Youngs, D. (1982). *Numerical methods for fluid dynamics*. New York American Press.

[59] Zuo, J., Xu, T., Zhu, D. Z., and Gu, H. (2022). Impact pressure of dam-break waves on a vertical wall with various downstream conditions by an explicit mesh-free method. *Ocean Engineering*, 256:111569.

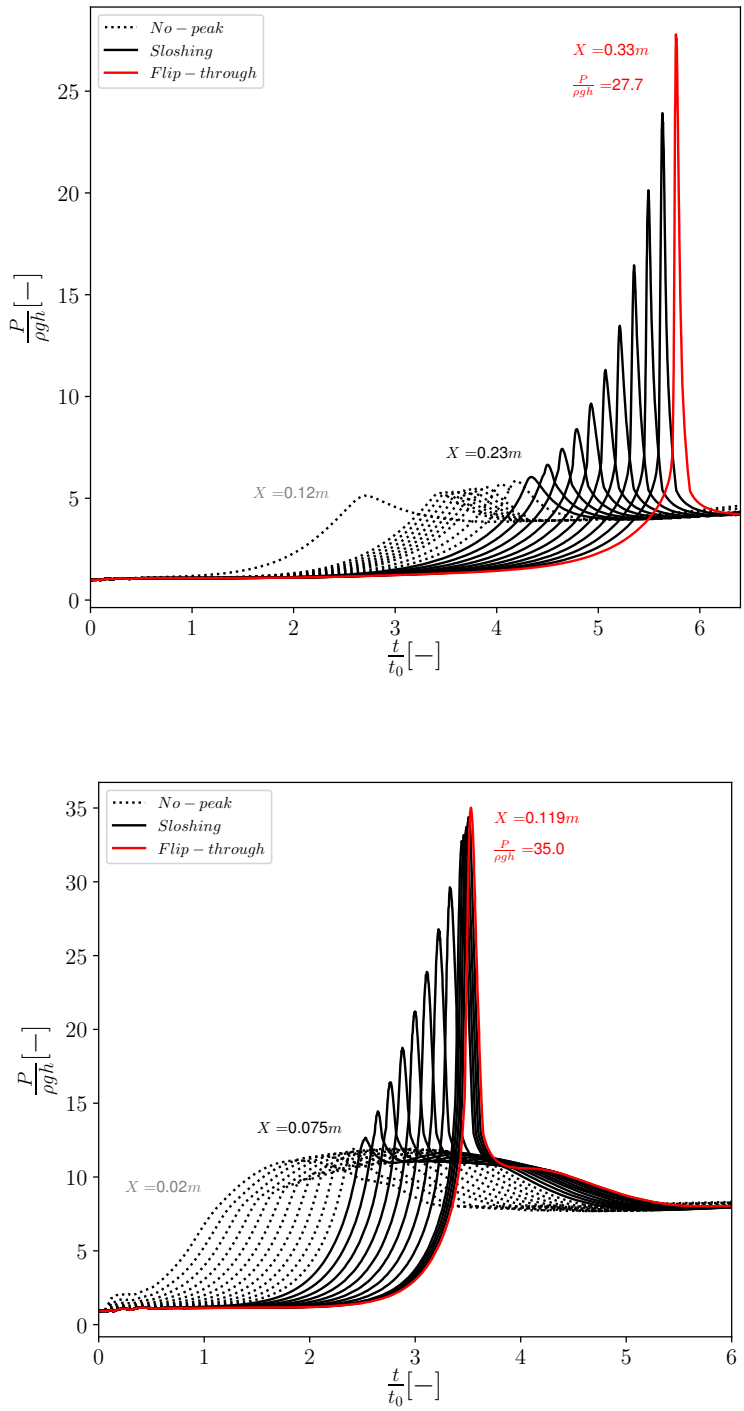

Figure 12: Evolution of the normalized pressure with relative time t/t_0 with $t_0 = h/c$, at elevation z_{pmax} for the reference cases $h = 18mm$ and $38mm$ (respective peak pressures are $6.185kPa$ and $10.36kPa$), gradually moving the obstacle to the right (i.e., varying X).

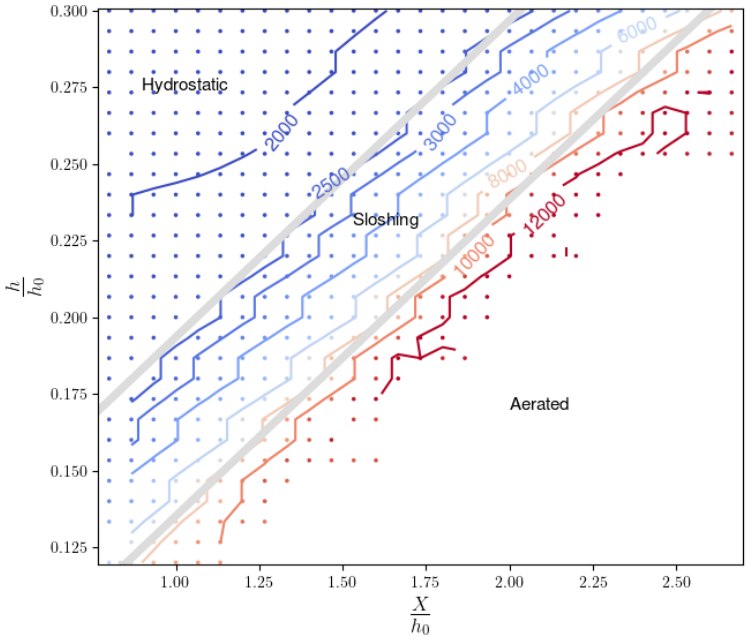

Figure 13: Contours of Max(P) in the scaled $X - h$ domain considering all the cases simulated

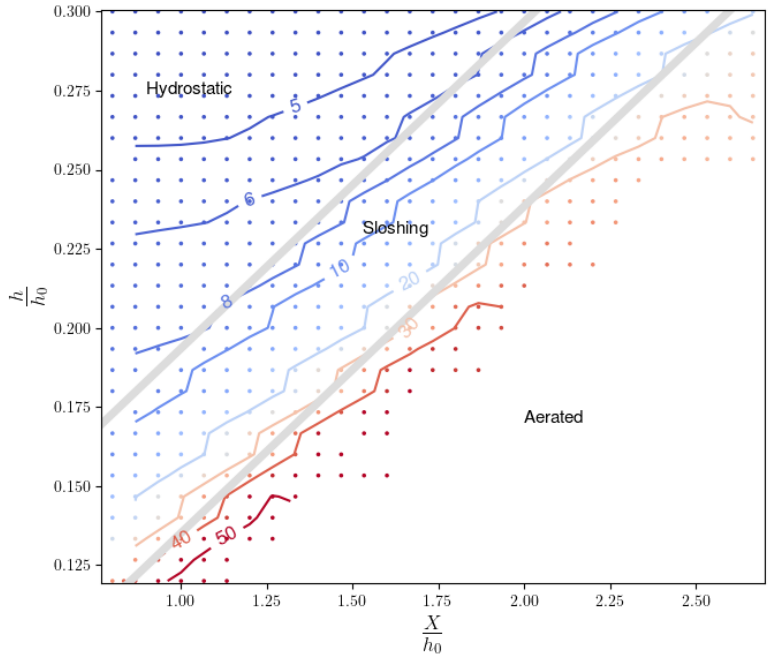

Figure 14: Contours of Max(P)/$\rho g h$ in the scaled $X - h$ domain

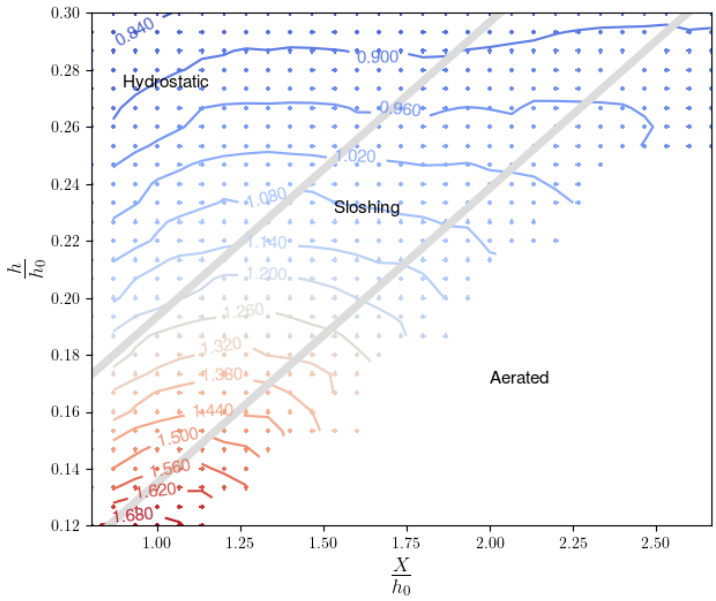

Figure 15: Contours of $V_{imp}/\sqrt{gh}$ in the scaled $X-h$ domain

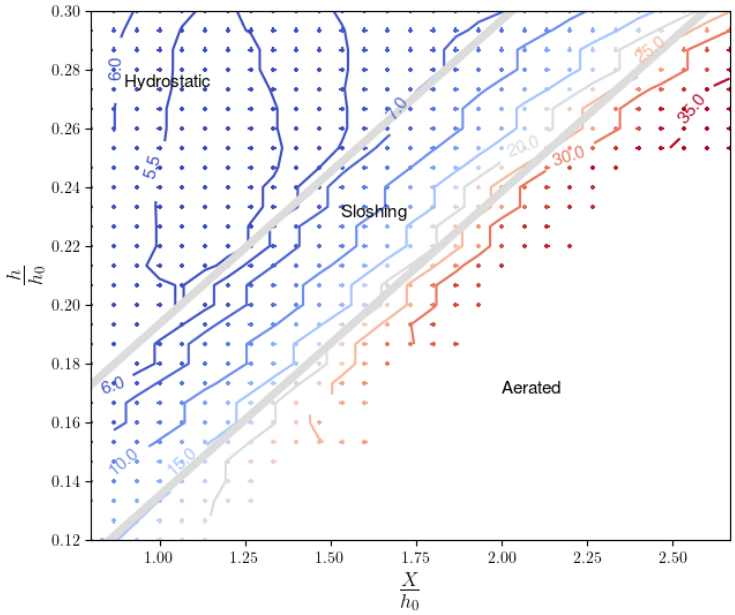

Figure 16: Contours of $\text{Max}(P)/\rho V_{imp}^2$ in the scaled $X - h$ domain

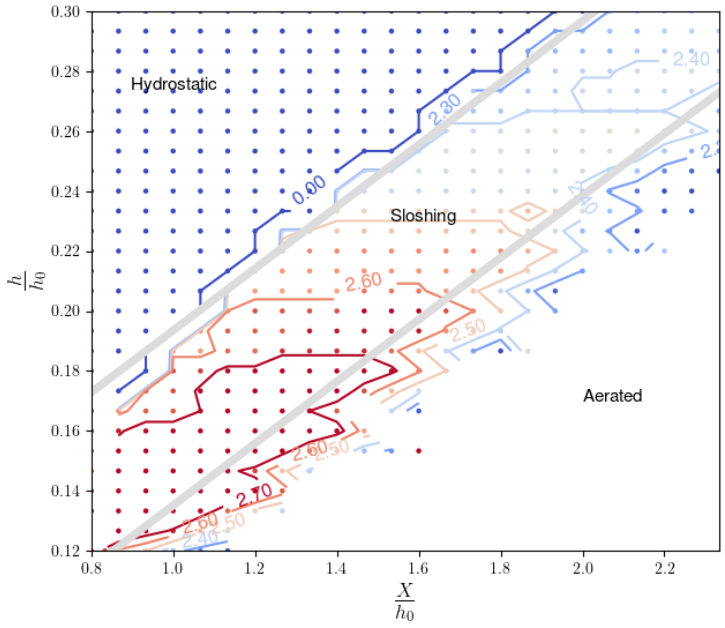

Figure 17: Contours of $z_{P_{max}}/h$ in the scaled $X - h$ domain

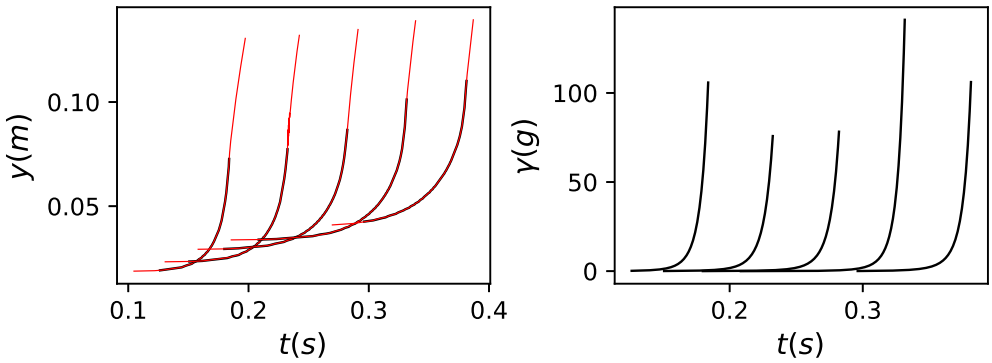

Figure 18: Left panel : free surface time evolution (red) next to the wall during the impact for X/h_0= 1 (first curve on the left and so on), 1.33, 1.66, 2, 2.33 and h/h_0=0.135, 0.17, 0.205, 0.24, 0.275 respectively. Right panel : corresponding accelerations in g calculated by fitting an exponential law on the black curves shown in the left panel and deriving twice.